CHAPTER II

LITERATURE REVIEW

The upcoming sections will provide insight into the quark-gluon plasma and the QCD phase diagram created by heavy-ion collision experiments. Additionally, it will cover the models utilized for the light nuclei production.

2.1 Heavy-ion collision

The main goals of heavy-ion collision experiments are to understand the nonperturbative aspects of QCD and create and probe a new state of matter called quark-gluon-plasma (QGP) which can be observed in collisions at sufficiently large center-of-mass energies (STAR Collaboration: J. Adams, 2005). In heavy-ion collisions, nuclei are accelerated to nearly the speed of light before they collide with each other. The time evolution of such a ultra high-energy collision usually is divided into four states as follows. First, thermalization occurs shortly after (~ 1 fm) the collision when a locally thermalized QGP is created, with quarks and gluons as relevant degrees of freedom. Second, during hadronization, hadrons begin to form out of the QGP medium. As time passes and the temperature decreases, the system reaches a state of chemical freeze-out. In this state, inelastic particle collisions cease, and no new particles are created, resulting in fixed particle multiplicities. The time evolution progresses to the final stage known as kinetic freeze-out, where elastic particle collisions come to an end, causing fixed particle spectra as they are measured by detectors (see figure 2.1).

In the beam energy regime where one expects to encounter a phase transition in QCD during the evolution such a schematic picture is not valid anymore. Most importantly, the initial compression phase, which is most sensitive on the underlying equation of state, cannot be treated independently from the bulk evolution. In addition the equilibrium phase and subsequent hadronic stage are highly intertwined. To be able to describe a phase transition in such a complex many body system the use of state-of-the-art microscopic transport simulations is necessary.

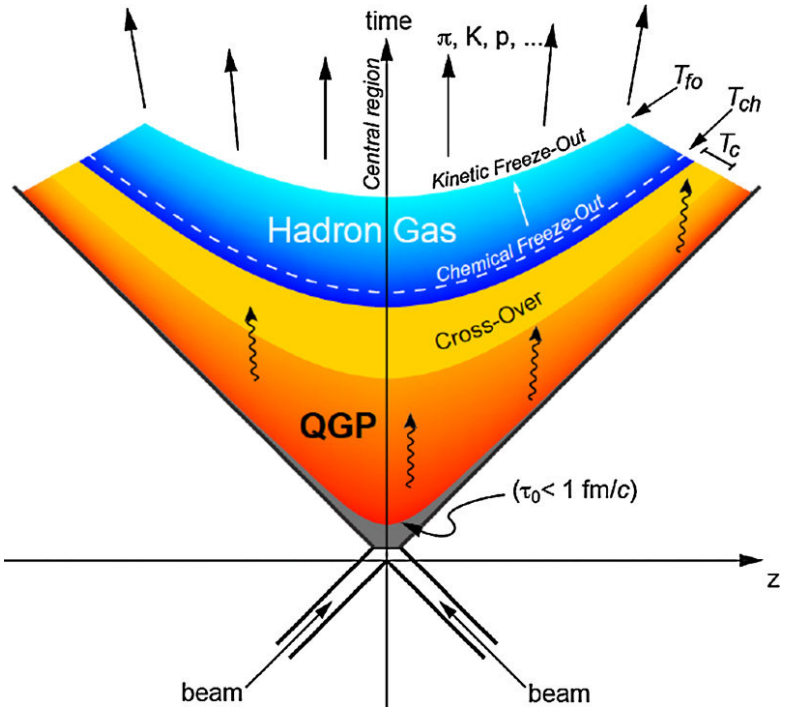

Figure 2.1 The space-time diagram of heavy-ion collision (Braun-Munzinger et al., 2019).

2.2 Quantum chromodynamics phase transition

The existence of a medium of deconfined quarks and gluons is expected at high temperature and/or density. As a consequence, this gives rise to an investigation of possible phase transition between confinement and deconfinement state as seen in the phase diagram of QCD (see figure 2.2).

As previously stated, during the hadronization process, the QGP matter undergoes the transition process, deconfined quarks are formed into hadronic matter. In heavy-ion collision experiments, the process of identifying a phase transition can be performed by several measurements through a variety of observables. These measurements, including fluctuations in particle counts (hadron multiplicities), their transverse momentum, and the mean transverse energy, serve as key indicators (Sasaki et al., 2007). Through an analysis of these fluctuations, one can effectively derive critical parameters such as the critical temperature and baryochemical potential from the equation of state as depicted within the Quantum Chromodynamics (QCD) phase diagram. Notably, as the critical point where the first-order phase transition terminates, these fluctuations are expected to be greatly enhanced. Experimentally, STAR (Abdallah et al., 2025), NA49/61 (Grebieszkow, 2009; Andronov, 2019), and for lowest energies, also the HADES

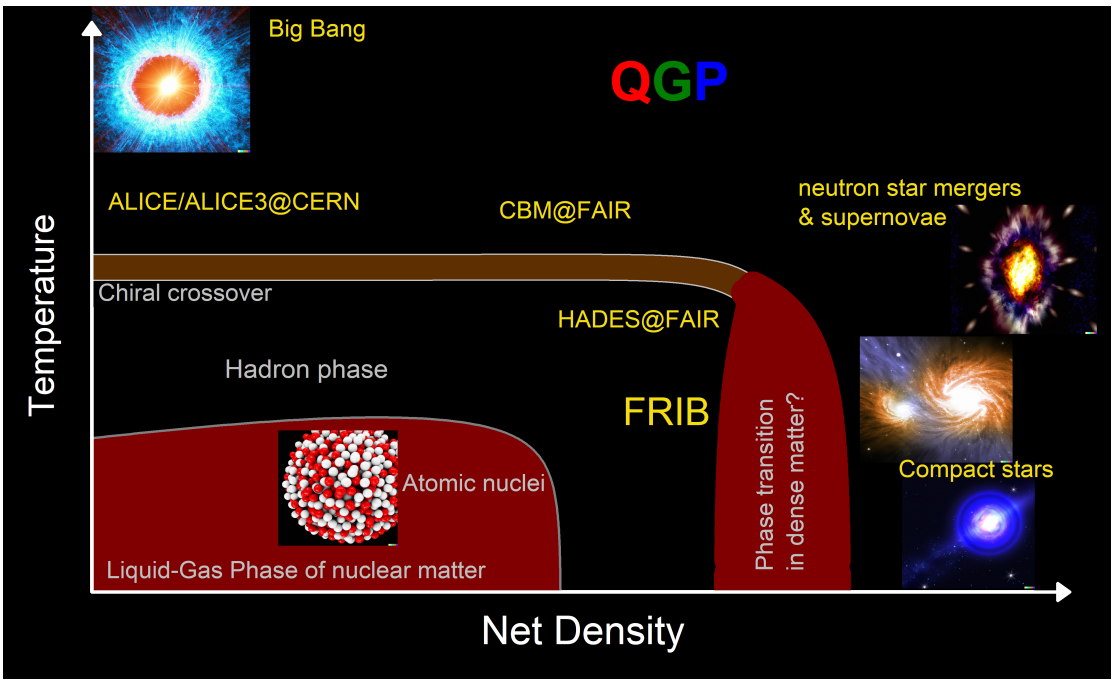

Figure 2.2 The phase diagram of quarks and gluons. The diagram displays the current knowledge and assumptions on possible states that quarks and gluons can become as function of temperature T and baryon density (image by Jan Steinheimer).

collaboration (Adamczewski-Musch et al., 2020) have provided data which so far have not been able to allow us a final conclusion about the existence of a QCD critical point and first-order phase transition.

Investigation of the phase transition in collision experiments can also be conducted through simulation models including chiral fluid dynamics. This is a model that accounts the QGP matter as a fluid undergoing a hydrodynamic expansion. The time evolution in the chiral order parameter implies a transition between chiral symmetry breaking and restoration. Entropy production (Herold, Kittiratpattana, et al., 2019) and enhancement in hadron multiplicity ratios have been identified as potential probes of a phase transition (Bumnedpan, Steinheimer, Bleicher, et al., 2022).

The order of the QCD transition for vanishing baryochemical potential has been unambiguously identified as a crossover rather than a phase transition using lattice QCD (Aoki et al., 2006). In this discretization of QCD on a lattice of finite volume, the QCD partition function can be computed directly, leading to the thermodynamic quantities sensitive to a phase transition like the chiral condensate as the potential order parameter or the chiral susceptibility.

As a consequence, a divergence of the susceptibility, in infinite matter, indicates the location of a phase transition (Karsch, 2017; Bazavov et al., 2020).

For finite chemical potential, lattice QCD suffers from the sign problem which makes direct calculations impossible. Alternative approaches include functional techniques using Dyson-Schwinger equations for the couple quark and gluon propagators (Fischer et al., 2014; Gao et al., 2021) or low-energy effective models, often base on the linear sigma or Nambu-Jona-Lasinio (NJL) models which both describe spontaneous chiral symmetry breaking by the QCD ground state (Scavenius et al., 2001; Schaefer et al., 2005; Fukushima, 2008). The location of the CEP has been estimated from functional techniques and also effective models, so far, however, with only little agreement between the various theoretical approaches.

2.3 Equation of state: EoS

An equation of state (EoS) is the relationship that links the various thermodynamics quantities, providing insight into how a macroscopic system behaves under different conditions. It is an essential input for any hydrodynamic model and contains information on the phase transition. For the purpose of heavy-ion collisions, we are going to introduce the grand canonical partition function

$$Z(T,V,\mu) = \sum_{N=0}^{\infty} \frac{1}{h^{3N}} \int d^{3N}x \int d^{3N}p \, \mathrm{e}^{\frac{-(H(x_\nu,p_\nu)-\mu N)}{T}} \, , \tag{1}$$

and the grand potential density

$$\Phi(T,V,\mu) = -\frac{T}{V} \ln Z = -P \, , \tag{2}$$

with the thermodynamics relation

$$\Phi(T,V,\mu) = \varepsilon - Ts - \mu n \, . \tag{3}$$

Here, ε, s, μ, and n represent energy density, entropy density, chemical potential, and particle number density, respectively.

In hyperspace, denoted by x_ν and p_ν, the positions and momenta are represented as $x_\nu = x_1, x_2, x_3, ..., x_N$ and $p_\nu = p_1, p_2, p_3, ..., p_N$, respectively. Here, H refers to the Hamiltonian. After determining the grand partition function, the mean particle number is can be calculated using the expression

$$\begin{aligned}\langle N\rangle &= \frac{1}{Z}\sum_{i=0}^{\infty} N\mathrm{e}^{\frac{-(E_i-\mu N)}{T}} = \left.\frac{\partial(T\ln Z)}{\partial\mu}\right|_{T,V} = -\left.\frac{\partial\Phi}{\partial\mu}\right|_{T,V} \\ &= \left.\frac{T}{Z}\frac{\partial Z}{\partial\mu}\right|_{T,V}. \end{aligned} \tag{4}$$

From now on, we will express all the quantities in natural units i.e., the Boltzmann constant $k = 1$.

For indistinguishable particles, the grand partition function becomes

$$\begin{aligned} Z(T,V,\mu) &= \sum_{i=0}^{\infty}\frac{1}{N!h^{3N}}\int d^{3N}x\int d^{3N}p\ \mathrm{e}^{-\frac{H-\mu N}{T}} \\ &= \sum_{i=0}^{\infty}(\mathrm{e}^{\mu/T})^N Z_c(T,V,N). \end{aligned} \tag{5}$$

Where $Z_c(T,V,N)$ is the canonical partition function. It can be seen that the grand partition function is weighted over the summation by a factor of $e^{\mu/T}$, this factor is later defined as the fugacity in which $e^{\mu/T} \equiv \lambda$.

In the context of non-interacting particles in a system, the expression of the canonical partition function can be rewritten in term of a partition function for one particle,

$$Z_c(T,V,N) = \frac{1}{N!}[Z_c(T,V,1)]^N. \tag{6}$$

The grand canocical partition function for non-interacting particles then becomes

$$
\begin{aligned}
Z(T,V,\mu) &= \sum_{N=0}^{\infty} \frac{1}{N!}(\mathrm{e}^{\mu/T})^N [Z_c(T,V,1)]^N \\
&= \sum_{N=0}^{\infty} \frac{1}{N!}(\lambda)^N [Z_c(T,V,1)]^N \\
Z(T,V,\mu) &= \mathrm{e}^{\lambda Z_c(T,V,1)}. \qquad (7)
\end{aligned}
$$

This form of the partition function can then be applied in a situation of relativistic ideal gas of identical particle. The Hamiltonian describing a relativistic ideal gas is expressed as

$$H = \sum_{i=0}^{N} E_i = \sum_{i=0}^{N} \sqrt{p_i^2 + m_i^2} \qquad (8)$$

Then the canonical function for one particle becomes

$$
\begin{aligned}
Z_c(T,V,1) &= \frac{1}{h^3} \int d^3x \int d^3p \, \mathrm{e}^{-\frac{\sqrt{p^2+m^2}}{T}} \\
&= \frac{V}{2\pi^2} \int_0^{\infty} p^2 dp \, \mathrm{e}^{-\frac{\sqrt{p^2+m^2}}{T}} \\
Z_c(T,V,1) &= \frac{V}{4\pi^2} \int_0^{\infty} \frac{m^3}{2} \sinh(t)\sinh(2t) e^{-\frac{m}{T}\cosh(t)} dt \qquad (9)
\end{aligned}
$$

The integral could be carried out by interchanging the variables: $\frac{p}{m} = \sinh(t)$ and $dp = m\cosh(t)$.

After determining the canonical partition function for a single particle, we can progress to calculate the grand partition function, Z, by applying the thermodynamic relationship as outlined in equation (3).

2.4 Correlations and fluctuations

The baryon number fluctuations arising from phase separation during a non-equilibrium first-order phase transition can be analyzed using the cumulants of multiplicity distributions within a fixed spatial volume. In this study, we focus on the cumulants C, which are closely related to the factorial cumulants employed in previous works (Skokov et al., 2013; Bzdak and Koch, 2019) and encapsulate essentially the same information. The first three cumulants are defined as follows:

$$C_1 = \langle N \rangle = \mu \tag{10}$$

$$C_2 = \sigma^2 = N^2 - \langle N \rangle^2 \tag{11}$$

$$C_3 = S\sigma^3 = \langle (N - \langle N \rangle)^3 \rangle \tag{12}$$

where μ is event averaged particle mean expectation value, S is the skewness and σ^2 is variance, the $\langle \cdot \rangle$ symbol denotes event-average quantity. In this work, we shall calculate the time dependence of proton number cumulants up to the 3rd order for beam energies 2.0 AGeV and 3.0 AGeV.

Given that cumulants scale linearly with system volume to first order, it is common practice to use their ratios to cancel out this volume dependence:

$$\frac{C_2}{C_1} = \frac{\sigma^2}{\mu} \tag{13}$$

$$\frac{C_3}{C_2} = S\sigma \tag{14}$$

The observed ratios are influenced by various features of the collision dynamics, not only by the presence of a phase transition. Three key factors that play a crucial role are fluctuations in the number of participants (Skokov et al., 2013), accurate handling of experimental acceptance, and corrections for experimental efficiency (Luo et al., 2019). In this study, we largely neglect these effects, as accurately accounting for them would demand detailed information about a specific detector setup, centrality determination procedure, and associated corrections. Instead, we focus on signals that remain visible even when volume fluctuations are included, assuming these are more likely to be experimentally observable. In contrast, signals that emerge only after substantial (and

sometimes model-dependent) corrections may not be entirely reliable.

2.5 Experimental results

As far as we have been mentioning the enhancements of the cluster as a signal for the phase transition from our simulation model, we now aim to show the cluster fluctuations via cumulant ratio observed at the relativistic heavy ion collider (RHIC) in the STAR collaboration experiment (see figure 2.3). Figure 2.3 shows the cumulant ratio C_4/C_2 for various collision systems, compared with results from UrQMD simulations. The data are consistent with the model employing an equation of state without a phase transition, further results are to be anticipated in the future compressed baryonic experiment at FAIR.

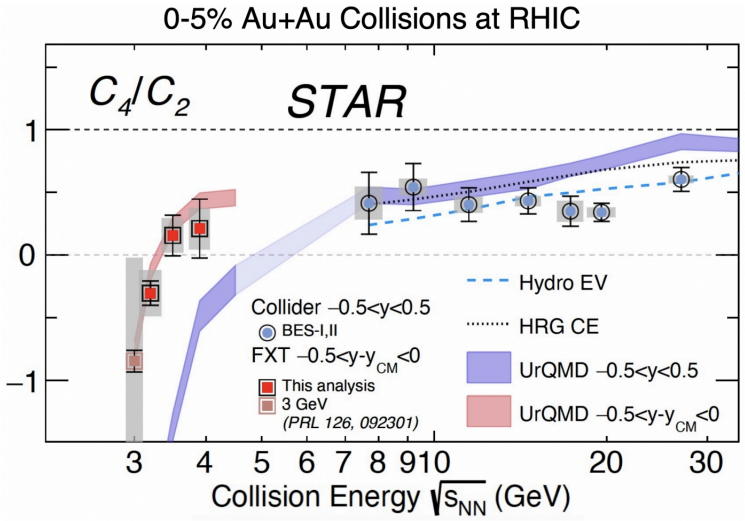

Figure 2.3 The proton cumulant ratio C_4/C_2 in two beam energy scan phases BES-I and BES-II at RHIC in different centralities under AuAu collision within rapidity range $|y| < 0.5$ (image taken from the Quark Matter 2025 in Frankfurt by Zachary Sweger, Wed, P35).

Another set of experimental results on the beam-energy-dependent cumulant ratios that we would like to represent comes from the STAR together with the HADES collaboration as displayed in figure 2.4. We hereby emphasize the result regarding the ratio K_3/K_2 (which is equivalent to $C_3/C_2 = S\sigma$ in this work). The data from STAR in the 0–5% centrality class (red circles), along with the 0–10% HADES data (red square), illustrate the trend of cumulant ratios across a wide range of collision energies—from the lowest accessible energies to the high-energy regime. Nevertheless, the data is still being collected and will be subject to further corrections in the upcoming CBM experiment.

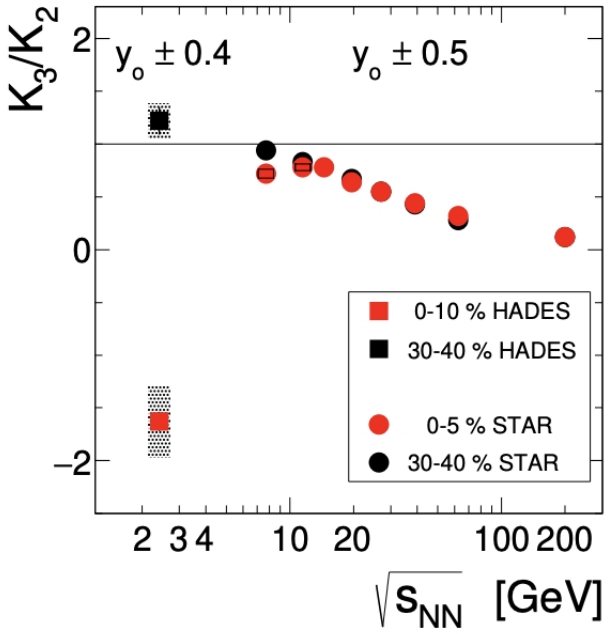

Figure 2.4 Beam energy dependence of the scaled cumulant K_3/K_2 in different centralities including a comparison with the STAR data (Adamczewski-Musch et al., 2020)

2.6 Light nuclei production

The production of the light nuclei: protons, deuterons, ^3He, and ^4He is employed as a probe for the first-order phase transitions. An enhanced light nuclei production as well as their double ratios implies a signal of the phase transition due to the emergence of local density fluctuations as the medium undergoes a dynamical first-order phase transition (Steinheimer and Randrup, 2012; Herold, Nahrgang, et al., 2014; Steinheimer, Randrup and Koch, 2014; Sun, Chen, Ko, Pu, et al., 2018; Sun, Ko, et al., 2021). With a focus on the result from (Sun, Ko, et al., 2021) in figure 2.5, the enhancement in the double ratio $(N_t * N_p)/d^2$ as a function of coupling strength g_V in the Lagrangian describing flavor-independent interaction of quarks. A peak structure can be clearly seen, indicating the first-order phase transition.

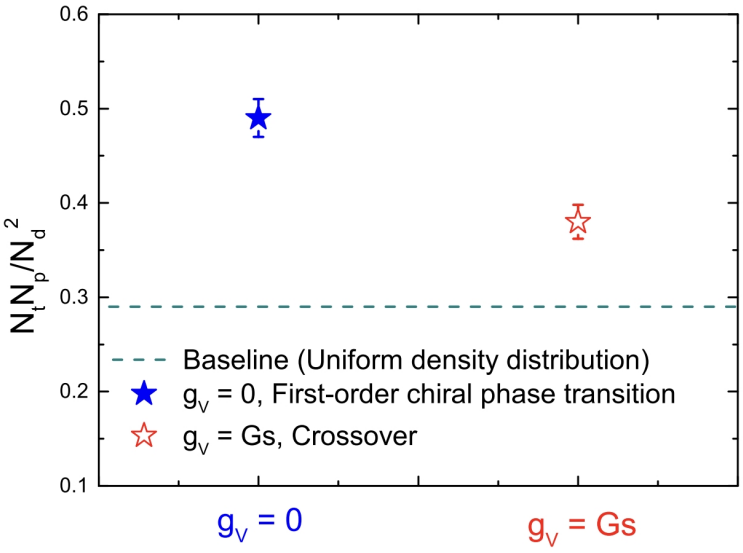

Figure 2.5 Double ratio of triton (t), proton (p) and deuteron (d) as a function of coupling strength with the case of first-order phase transition (blue solid star) and crossover (red open star) (Sun, Ko, et al., 2021)

The following sections will provide a further explanation of the model regarding the production of the light nuclei.

2.6.1 Coalescence model

The formation of nuclei can be described by the coalescence model (Sun, Chen, Ko and Xu, 2017), a phenomenological model of light nuclei formation after the kinetic freeze-out. The concept of light nuclei formation involves the merging of protons and neutrons with nearly identical momentum and positions, defined by cutoff values for relative momenta and positions.

Our research focuses on understanding of the QCD first-order phase transition as it is expected to occur in the QCD phase diagram for large values of the baryochemical potential and, consequently, low to intermediate energies in heavy-ion collision experiments. As a potential signal for a first-order transition, we are mainly interested in the light nuclei production.

The momentum-space coalescence is a way to describe how particles with specific momenta come together to form larger particles or clusters based on their momentum characteristics. The expression of momentum-space coalescence is given

by (Dover et al., 1991)

$$N_c = g_c \int \left(\prod_{i=1}^{N} dN_i \right) f_c^W(\overrightarrow{r}_1, \cdots, \overrightarrow{r}_N, \overrightarrow{p}_1, \cdots, \overrightarrow{p}_N) \ , \tag{15}$$

where $f_c^W(\overrightarrow{r}_1, \cdots, \overrightarrow{r}_N, \overrightarrow{p}_1, \cdots, \overrightarrow{p}_N)$ is the Wigner function which is proportional to the coalescence probability, and g_c is the coalescence factor.

2.6.2 Thermal model

The thermal model, also known as the statistical model, is a model used to calculate the particle production yield (multiplicity) at the chemical freeze-out by assuming an equilibrated global heat bath out of which all particles are produced at a common temperature T, volume V, and baryochemical potential μ_B. The logarithm of the grand canonical partition function of particle species i is expressed in the form

$$\ln Z_i = \begin{cases} \dfrac{V g_i}{2\pi^2} \displaystyle\int_0^\infty p^2 dp \, \ln\left(1 + \lambda_i \mathrm{e}^{-E_i/T}\right) \text{ for fermions} \ , \\ \\ \dfrac{-V g_i}{2\pi^2} \displaystyle\int_0^\infty p^2 dp \, \ln\left(1 - \lambda_i \mathrm{e}^{-E_i/T}\right) \text{ for bosons} \ , \end{cases} \tag{16}$$

with $\mu_i = B_i\mu_B + S_i\mu_s + Q_i\mu_Q$, the chemical potential of particle species i being expressed as a linear combination of the chemical potential of a certain quantity as follows: B for baryon number, S for strangeness and Q for electric charge. Here, $\lambda_i = e^{\mu_i/T}$ is the fugacity of particle species i, g_i is the degeneracy, and E_i denotes the relativistic energy. With a known partition function, the pressure and the particle number density can be calculated,

$$P_i = \frac{T}{V}\ln Z_i = \begin{cases} \dfrac{Tg_i}{2\pi^2}\displaystyle\int_0^\infty p^2 dp \ln\left(1+\lambda_i \mathrm{e}^{-E_i/T}\right) & \text{for fermions ,} \\ \dfrac{-Tg_i}{2\pi^2}\displaystyle\int_0^\infty p^2 dp \ln\left(1-\lambda_i \mathrm{e}^{-E_i/T}\right) & \text{for bosons ,} \end{cases} \tag{17}$$

$$n_i = \frac{\partial P_i}{\partial \mu_i} = \begin{cases} \dfrac{g_i}{2\pi^2}\displaystyle\int_0^\infty \frac{p^2 dp}{1+\mathrm{e}^{(E_i-\mu_i)/T}} & \text{for fermions ,} \\ \dfrac{g_i}{2\pi^2}\displaystyle\int_0^\infty \frac{p^2 dp}{1-\mathrm{e}^{(E_i-\mu_i)/T}} & \text{for bosons .} \end{cases} \tag{18}$$

To eliminate the dependence on the source volume V as an additional fit parameter to the thermal model, particle number ratios are often used rather than absolute numbers,

$$\frac{N_i}{N_j} = \frac{n_i V}{n_j V} = \frac{n_i}{n_j}. \tag{19}$$

With this relationship, experimental measurements of particle number ratios can be compared with the model's predictions. The thermal model has successfully reproduced hadron and light nuclei yields over a wide range of beam energies and experiments (Albright et al., 2015; Biswas, 2020; Bhattacharyya et al., 2021).

2.7 Fluctuations in coordinate vs. momentum space

Density fluctuations in coordinate space arise from local variations in energy, pressure, or temperature during heavy-ion collisions. These fluctuations may result from phase transitions or inhomogeneities in the initial conditions. Effects such as collective flow and particle rescattering can dilute or distort the original fluctuation patterns. Nevertheless, the signals can become more pronounced under certain conditions, particularly when fluctuations occur near the freeze-out stage or when the medium exhibits low viscosity. Observables such as higher-order cumulants (e.g., $S\sigma$ and $K\sigma^2$) and particle yield ratios involving light nuclei are especially sensitive to these effects.

The result of a relation between the corrected scaled variance of the particle number within the rapidity acceptance and the fixed acceptance fraction (Kuznietsov et al., 2024) has shown that the limiting cases for the result in coordinate space can only be consistent with high collision energy $\sqrt{s_{NN}} = 5,020$ GeV (see figure 2.6).

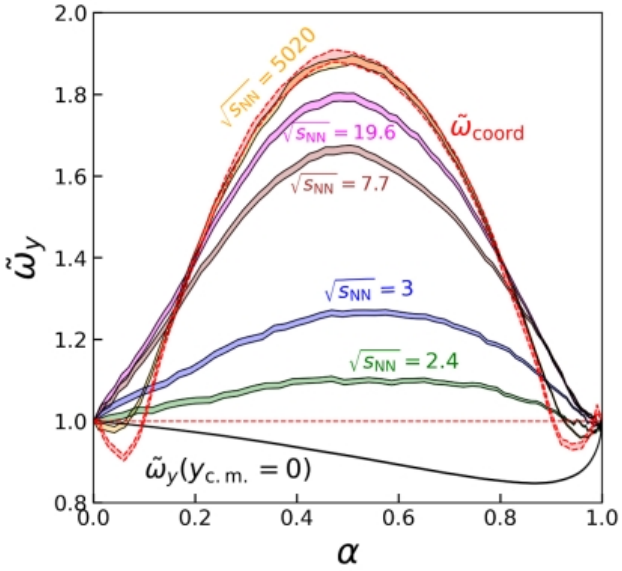

Figure 2.6 Corrected scaled variance $\tilde{\omega}_y$ as a function of fixed acceptance fraction α_y. The bands correspond to the beam energies $\sqrt{s_{NN}}$. The limiting cases of coordinate space are shown in red band, labeled $\tilde{\omega}_{coord}$ (Kuznietsov et al., 2024).